IEEE Access
Multidisciplinary | Rapid Review | Open Access Journal

Received 13 March 2024, accepted 19 March 2024, date of publication 22 March 2024, date of current version 28 March 2024.

Digital Object Identifier 10.1109/ACCESS.2024.3380849

RESEARCH ARTICLE

Influence of Concentric and Unequal-Turn Windings on Vibration of Induction Machines Considering Supply With Low-Order Harmonics

XUANDONG WU[1], LIMIN DIAO[2], ZIXU WANG[3], (Student Member, IEEE), SHAN WANG[4], AND HAISEN ZHAO[3], (Senior Member, IEEE)

[1]Wolong Electric Nanyang Explosion Group Company Ltd., Nanyang, Henan 473008, China
[2]Harbin Electric Power Equipment Company Ltd., Harbin, Heilongjiang 150066, China
[3]State Key Laboratory of Alternate Electrical Power System with Renewable Energy Sources, North China Electric Power University (NCEPU), Beijing 102206, China
[4]Dezhou Hengli Electrical Machinery Company Ltd., Dezhou, Shandong 253011, China

Corresponding author: Haisen Zhao (zhaohisen@163.com)

This work was supported in part by the National Natural Science Foundation of China under Grant 52177041.

ABSTRACT As the wide application of power electronics devices, supply containing low-order harmonic becomes more and more common in industry. It may cause the significant vibration of induction motors (IMs). This study firstly analyzed the time-space distribution characteristics of the additional electromagnetic force caused by the low-order harmonics in supply. Then, an improved concentric and unequal-turn windings is designed and its impact on unconventional vibration of IMs is also analyzed. The increase ratio of force amplitude between the force in different cases is defined, by which the force characteristics of IMs with supply containing low-order harmonics and concentric and unequal-turn windings can be revealed under different load conditions. With a 32-kW IM, harmonic response analysis and experimental validation are also carried out, the results show that, with concentric unequal-turn winding, the vibration in different frequency bands can be reduced effectively, the average vibration can be suppressed from 89.7dB to 86.9dB.

INDEX TERMS Induction motors (IMs), electromagnetic force, concentric and unequal-turn windings, vibration.

I. INTRODUCTION

Due to the wide application of power electronic devices in power system, the power quality problem, especially for harmonic in power grid becomes more and more prominent. Induction motors (IMs), as the largest proportion of energy consumption equipment, harmonic pollution in supply inevitably causes unconventional vibration and noise of IMs and reduces service life. Therefore, it is necessary to study the influence of harmonic supply on unconventional vibration characteristics of IMs and put forward corresponding suppression measures.

Since 1990s, many studies focused on motor vibration mechanism, such as the distribution of transient field [1], analytical model of radial electromagnetic force and its relationship with electromagnetic vibration of motor [2], and vibration response analysis based on magnetic circuit model of motor [3]. However, the previous research on electromagnetic force just focuses on the time harmonic analysis with fixed spatial sampling points [4], [5], it is difficult to fully revealing the excitation mechanism and distribution characteristics of electromagnetic force. Meanwhile, the vibration spectrum of IMs is closely related to the harmonic components in supply [6]. Considering harmonic current's phase sequence, phase angle, frequency, and other parameters on electromagnetic force, especially for the low-order ones, the relation between harmonic current and electromagnetic force

The associate editor coordinating the review of this manuscript and approving it for publication was Pinjia Zhang.

with some special orders is constructed [7], and the intrinsic relationship between power frequency and double power frequency [8], [9]. However, there are still lack of models and analytical methods that can completely coverage the vibration mechanism caused by harmonic current. Based on the analysis of the space-time distribution of electromagnetic force, a series of studies have been conducted on the impact of the motor ontology optimization method on vibration characteristics. For instance, new skewed rotors can reach remarkable effect of performance of vibration, such as zigzag skew pole [10] and multi-skewed rotor [11], [12] which can reduce the amplitude of radial electromagnetic force and avoid the additional torque effectively compared with the conventional skewed rotor; Furthermore, after applying the low harmonic winding, such as short pitch winding [13], fractional slot concentrated winding [14], [15], [16], [17] and concentric and unequal-turn winding [18], [19], the sinusoidal characteristics of the spatial distribution of magnetomotive force (MMF) are more prominent, so the harmonic content of MMF can be greatly reduced. Due to the existence of reverse MMF in the analytic model, the refined analysis model of electromagnetic force is still unclear in the process of application of low harmonic winding.

The previous studies mainly focus on refining vibration models precisely and developing multiple suppression measures coordinatively. However, the current studies are still lack of analysis on characteristics of motor vibration caused by low-order harmonic in supply; meanwhile, the influence of concentric and unequal-turn windings on the unconventional vibration caused by low-order harmonic should also be further investigated to develop low-cost and high-efficiency vibration reduction measurement.

To solve these problems, this study firstly analyzes the air-gap flux density and the related electromagnetic force considering cross coupling between the supply with low-order harmonics and different time-space harmonics of IMs, the low-order force caused by the low-order harmonics is also highlighted, which may affect vibration performance of IMs significantly. Meanwhile, a cost-effective concentric and unequal-turn windings is proposed and the influence on vibration characteristics is researched through finite element analysis (FEA). Finally, experimental validation was performed on a 32-kW IM, the result shows that the average vibration level can be suppressed from 89.7dB to 86.9dB.

II. ELECTROMAGNETIC FORCE OF IMS CONTAINING LOW-ORDER HARMONICS IN SUPPLY

A. AIR-GAP FLUX DENSITY CAUSED BY HARMONIC CURRENT WITHOUT SLOTTING EFFECT

Fundamental MMF induced by *n-th* order harmonic current in three-phase winding can be deduced in (1).

$$\begin{aligned} f_{n-1}(\theta,t) &= f_{n-A1}(\theta,t)+f_{n-B1}(\theta,t)+f_{n-C1}(\theta,t) \\ &= \frac{3}{2}F_{\varphi n-1}\cos(p\theta-n\omega_1 t) \\ &= F_{n-1}\cos(p\theta-n\omega_1 t) \end{aligned}$$

$$\begin{aligned} F_{n-1} &= 1.35\frac{N}{p}I_n k_{w1} \\ n &= 2m_1 k\pm 1 \quad k=0,1,2\ldots\ldots \end{aligned} \tag{1}$$

where n is the order of harmonic current and m_1 is the number of phases, $f_{n-1}(\theta,\mathrm{t})$ is the fundamental MMF induced by the *n-th* harmonic current, $f_{n-A1}(\theta,t)$, $f_{n-B1}(\theta,t)$ and $f_{n-C1}(\theta,t)$ are the fundamental MMF induced by the *n-th* harmonic current in three-phase windings, respectively; F_{n-1} is the amplitude of three-phase synthetic MMF, N is the number of winding turns, p is the pole pair of the motor, ω_1 is the fundamental angular frequency, I_n is the effective value of *n-th* harmonic current, k_{w1} is the winding coefficient.

Moreover, the spatial harmonic MMF caused by *n-th* harmonic current can also be deduced as in (2).

$$\begin{aligned} \sum_{\gamma}^{\infty} f_{n-\gamma}(\theta,t) &= \sum_{\gamma}^{\infty} f_{n-A\gamma}(\theta,t)+\sum_{\gamma}^{\infty} f_{n-B\gamma}(\theta,t) \\ &\quad +\sum_{\gamma}^{\infty} f_{n-C\gamma}(\theta,t) \\ &= \frac{3}{2}\sum_{\gamma}^{\infty} F_{\varphi n-\gamma}\cos(\gamma p\theta\pm n\omega_1 t) \\ &= \sum_{\gamma}^{\infty} F_{n-\gamma}\cos(\gamma p\theta\pm n\omega_1 t) \\ F_{n-\gamma} &= 1.35\frac{N}{\gamma p}I_n k_{w\gamma} \end{aligned} \tag{2}$$

where $f_{n-\gamma}(\theta,t)$ is the harmonic MMF induced by the *n-th* harmonic current, $f_{n-A\gamma}(\theta,t)$, $f_{n-B\gamma}(\theta,t)$ and $f_{n-C\gamma}(\theta,t)$ are the harmonic MMF induced by the *n-th* harmonic current in three-phase winding, respectively; $F_{n-\gamma}$ is the amplitude of three-phase synthetic MMF, γ is the harmonic order of MMF, $k_{w\gamma}$ is the harmonic winding coefficient. Based on the above analysis, the MMF induced by each harmonic current in three-phase symmetrical winding can be expressed as in (3).

$$f(\theta,t)=\sum_{n}\sum_{\gamma}F_{n-\gamma}\cos(\gamma p\theta\pm n\omega_1 t) \tag{3}$$

Ignoring the harmonic permeability caused by slotting effect, the air-gap flux density considering harmonic current in supply can be obtained as in (4).

$$\begin{aligned} b(\theta,t) &= b_1(\theta,t)+b_\nu(\theta,t)+b_r(\theta,t)+b_{n-1}(\theta,t) \\ &\quad +b_{n-\gamma}(\theta,t) \\ &= B_1\cos(p\theta-\omega_1 t-\varphi_{1r}) \\ &\quad +\sum_{\nu}B_\nu\cos(\nu\theta-\omega_1 t-\varphi_{\nu r}) \\ &\quad +\sum_{\mu}B_\mu\cos(\mu\theta-\omega_\mu t-\varphi_\mu) \\ &\quad +\sum_{n}B_{n-1}\cos(p\theta-n\omega_1 t-\varphi_{nr}) \\ &\quad +\sum_{n}\sum_{\gamma}B_{n-\gamma}\cos(\gamma p\theta\pm n\omega_1 t-\varphi_{\gamma r}) \end{aligned} \tag{4}$$

where $b(\theta, t)$ is air-gap flux density, $b_1(\theta, t)$ and $b_v(\theta, t)$ are the fundamental and *v-th* harmonic components under sinusoidal supply, respectively; $b_r(\theta, t)$ is the flux density caused by rotor current, ω_μ is the angular frequency, $b_{n-1}(\theta, t)$ and $b_{n-\gamma}(\theta, t)$ are the fundamental MMF induced by harmonic current in supply and the additional flux density generated by harmonic MMF. B_1, B_v, B_μ, B_{n-1} and B_{n-v} are the amplitude of each flux density component; $\varphi_{1r}, \varphi_{vr}, \varphi_\mu, \varphi_{nr}$ and $\varphi_{\gamma r}$ are the phase difference of the above components.

B. RADIAL ELECTROMAGNETIC FORCE WITH HARMONIC SUPPLY

Generally, the high order, small amplitude and constant components of the radial electromagnetic force can be ignored, due to faint influence on vibration. Then, radial electromagnetic force considering harmonic supply [20], [21] is as in (5).

$$
\begin{aligned}
p_r(\theta, t) &= \frac{b^2(\theta, t)}{2\mu_0} \\
&\approx \frac{1}{2\mu_0}\Bigg\{
\begin{aligned}
&\frac{B_1^2}{2}\cos(2p\theta - 2\omega_1 t - 2\varphi_{1r}) \\
&+\sum_{v}\sum_{\mu} B_\mu B_v \cos[(\mu \pm v)p\theta \\
&\quad -(\omega_\mu \pm \omega_1)t - (\varphi_{vr} \pm \varphi_\mu)] \\
&+\sum_{n} B_1 B_{n-1}\cos[2p\theta - (n+1)\omega_1 t \\
&\quad -(\varphi_{nr} + \varphi_{1r})] \\
&+\sum_{n}\sum_{\gamma} B_1 B_{n-\gamma}\cos[(\gamma \pm 1)p\theta \\
&\quad -(n\omega_1 \pm \omega_1)t - (\varphi_{\gamma r} \pm \varphi_{1r})] \\
&+\sum_{v}\sum_{n} B_v B_{n-1}\cos[(1 \pm v)p\theta \\
&\quad -(n\omega_1 \pm \omega_1)t - (\varphi_{nr} \pm \varphi_{vr})] \\
&+\sum_{v}\sum_{n}\sum_{\gamma} B_v B_{n-\gamma}\cos[(\gamma \pm v)p\theta \\
&\quad -(n\omega_1 \pm \omega_1)t - (\varphi_{\gamma r} \pm \varphi_{vr})] \\
&+\sum_{n}\sum_{\mu} B_\mu B_{n-1}\cos[(\mu \pm 1)p\theta \\
&\quad -(\omega_\mu \pm n\omega_1)t - (\varphi_{nr} \pm \varphi_\mu)] \\
&+\sum_{n}\sum_{\gamma}\sum_{\mu} B_\mu B_{n-\gamma}\cos[(\mu \pm \gamma)p\theta \\
&\quad -(\omega_\mu \pm n\omega_1)t - (\varphi_{\gamma r} \pm \varphi_\mu)]
\end{aligned}
\end{aligned}
\tag{5}
$$

where $p_r(\theta, t)$ is the radial electromagnetic force considering the harmonic supply, μ_0 is the vacuum permeability. The fundamental and harmonic flux density generated by the harmonic current are coupled with the original flux density respectively as additional electromagnetic force. Therefore, the force in (5) can be divided into four categories: 1) The force excluding the influence of low-order harmonic current; 2) The force induced by low-order harmonic current and fundamental flux density; 3) The force coupled by low-order harmonic current and harmonic MMF caused by fundamental current in stator winding; 4) The force induced by low-order current harmonic and harmonic MMF caused by rotor current.

TABLE 1. Space-Time Order of Force Excluding the Influence of Low-Order Harmonic Current.

Harmonic order	Space/Time multiplier			
	γ	v		
μ	1	1	-5	7
1	$p/2$	$p/2$ 0/0	-2p/8 ---	--- ---
-5		-2p/4 ---	--- 0/0	-p/10 ---
7		---	p/14	---
		---	---	0/0

TABLE 2. Space-Time Order of Force Induced by Low-Order Harmonic Current and Fundamental Flux Density.

Harmonic order	Space/Time multiplier		
	n		
γ	5	7	11
1	$p/6$	$p/8$	$p/12$
-5	2p/6	-2p/8	-2p/12

The above analysis method is based on the coupling effect of the incremental flux density introduced by low-order supply harmonic and the original flux density, which is theoretically suitable for other types of motors, The external deformation of the stator is approximately inversely proportional to the 4th power of the space order of the electromagnetic force and the force component less than space order 4 are often taken as the main research object [22]. Tables 1 to 4 involve the coupling results of 4 types of incremental flux densities in equation (4) in the range of phase band harmonics respectively. Only the radial electromagnetic force with space order 0-4th are involved. In the table, the parameters on the left side of "/" correspond to the space order, the other side correspond to the time order, and "—" corresponds to the force components with space order more than 4th, the subsequent analysis of which is not involved.

Based on (5), In the range of phase band harmonics, the radial force with low-order harmonic current in supply does not introduce new spatial order compared with the radial force with sinusoidal supply. The spatial order is concentrated in the 0, 2, -4, and the frequency is in the range of 0 to 1200Hz. The following part explore the law of important order force with low-harmonic current in supply from the perspective of force decomposition and the suppression of vibration and noise by using a novel concentric and unequal-turn winding is analyzed.

TABLE 3. Time-Space Order of Force Coupled by Low-Order Harmonic Current and Harmonic MMF Caused by Fundamental Current in stator winding.

Harmonic order	Space/Time multiplier			
	γ	n		
ν		5	7	11
1	---	p/6	p/8	p/12
		0/4	0/6	0/10
-5		-2p/6	-2p/8	-2p/12
ν	γ	5	7	11
1	-5	-2p/6	-2p/8	-2p/12
-5		0/4	0/6	0/10
7		p/6	p/8	p/12
ν	γ	5	7	11
-5	7	p/6	p/8	p/12
7		0/4	0/6	0/10

TABLE 4. Space-Time Order of Force Induced by Low-Order Current Harmonic and Harmonic MMF Caused by Rotor Current.

Harmonic order	Space/Time multiplier			
	γ	n		
μ		5	7	11
1	---	p/6	p/8	p/12
		p/12	p/14	p/18
		p/0	p/2	p/6
		0/4	0/6	0/10
		0/2	0/0	0/4
		0/10	0/12	0/16
-5		-2p/0	-2p/2	-2p/6
		-2p/6	-2 p /8	-2p/12
		2p/6	2p/4	2p/0
μ	γ	5	7	11
1	-5	-2p/6	-2p/8	-2p/12
		-2p/12	-2p/14	-2p/18
		-2p/0	-2p/2	-2p/6
-5		0/10	0/12	0/16
		0/4	0/6	0/10
		0/6	0/18	0/22
7		p/12	p/14	p/18
		p/18	p/20	p/24
		p/6	p/8	p/12
μ	γ	5	7	11
-5	7	p/0	p/2	p/6
		p/6	p/8	p/12
		-p/6	-p/3	p/0
7		0/2	0/0	0/4
		0/8	0/6	0/2
		0/4	0/6	0/10

III. CONCENTRIC AND UNEQUAL-TURN WINDING BASED ON MINIMUM HARMONIC COEFFICIENT

A. CONCENTRIC AND UNEQUAL-TURN WINDING

The above analysis shows that the low-order supply harmonics can be coupled with the other flux densities to induce a variety of electromagnetic forces, especially many low-order forces. Therefore, how to implement low-cost and high-efficient vibration reduction scheme is concerned in industrial application. The low-harmonic winding, by changing the spatial arrangement of conductor in each stator slot can effectively suppress the harmonic MMF and the harmonic flux density can be effectively suppressed to a certain extent to suppress motor vibration. However, how to reasonably determine the optimal number of turns of low-harmonic winding and the influence of vibration characteristic in different frequency bands considering low-order harmonics in supply need to be further investigated. Therefore, a 32-kW IM is adopted and the details are shown in Table 5.

TABLE 5. Detials of 32-kW IM.

Parameters	Value
Rated power (kW)	32
Rated speed (rpm)	1480
Rated voltage (V)	380
Number of poles	4
Numbers of stator/rotor slots	48/60
Diameter of stator (mm)	368/245
Diameter of rotor (mm)	80

The design principle of the concentric and unequal-turn winding is that the number of conductors in the slots is properly distributed, so that the current in the slots is distributed along the surface of the core according to the sinusoidal distribution, the MMF curve closer to the sinusoidal distribution can also be obtained. The design method is contrary to the analysis method, using the current layer distributed along the inner circle of the stator according to the sinusoidal curve, the slot current at each slot position is calculated, and the slot current ratio in each slot of each phase is calculated. The design scheme of concentric and unequal-turn winding follows three steps: 1) basic parameter calculation. 2) coefficient comparison check. 3) final design scheme determination. The design flow chart of concentric and unequal-turn windings is shown in Fig.1. The number of slots per phase in each stage of the motor involved in this paper is 4, and the electrical Angle of the slot is 15, the corresponding current layer and induced MMF waveform are shown in Figure 2.

B. DESIGN CRITERION OF CONCENTRIC AND UNEQUAL-TURN WINDING

The harmonic coefficients of original winding and three types of improved winding schemes are shown in Table 6 respectively. The scheme 2 has the best weakening effect for the 5th and 7th harmonics, therefore, scheme 2 is taken as the final scheme to study the suppression of unconventional vibration containing low harmonic in supply. The parameters of the original winding and the scheme 2 are shown in Table 7. The distribution of ordinary and scheme 2 are shown in Fig.3.

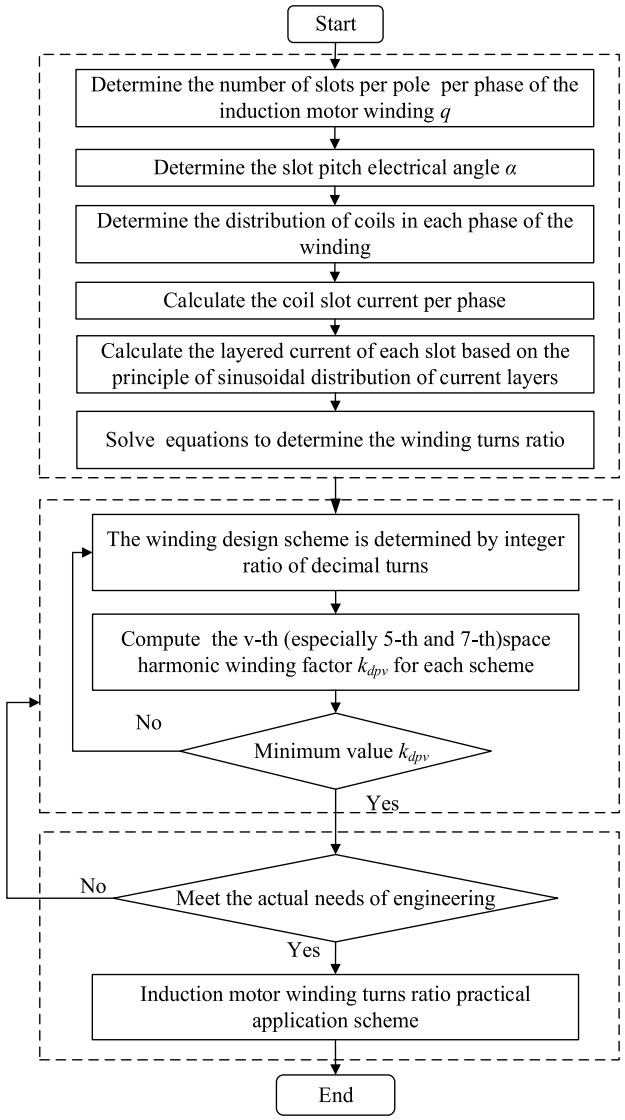

FIGURE 1. Design flow chart of concentric and unequal-turn winding.

TABLE 6. Winding Coefficients of Different Schemes.

Harmonic order	Winding scheme			
	Original	Scheme1	Scheme2	Scheme3
1	0.9495	0.9250	0.9024	0.9142
5	0.1629	0.0531	0.0089	0.0579
7	0.0959	0.0408	0.0398	0.0757
11	0.0165	0.1218	0.0204	0.0108
13	0.0165	0.1218	0.0204	0.0108

The two layers of conventional winding are arranged with equal turns, and concentric and unequal-turn windings is arranged according to the turn ratio of 6:4:3:1.

TABLE 7. Main parameters of the winding design schemes.

Winding design scheme	Turns per slot (ratio)	Pitch
Ordinary scheme	7	11
Low-harmonic scheme	6:4:3:1	11:9:7:5

IV. VIBRATION CHARACTERISTICS OF IMS WITH CONCENTRIC AND UNEQUAL-TURN WINGDING

The type of vibration studied is transverse vibration, tangential and torsional vibration characteristics are not considered. In addition, to be consistent with the actual condition of the field test result, only no-load and full-load conditions of the motor are analyzed. According to the above-mentioned winding scheme, three FEA cases of 32-kW, 4-pole IM are carried out, including:

1) Case#1: sinusoidal supply and application of conventional winding;

2) Case#2: supply containing low-order harmonic and application of conventional winding;

3) Case#3: supply containing low-order harmonic and application of concentric unequal-turn winding.

To compare Case#1 and Case#2, the force increment ratio η_{inc} is introduced to represent the increase of the amplitudes of all the electromagnetic force components mentioned in Table 1-4 when the power supply contains low-order harmonic; To compare Case#2 and Case#3, the force inhibition ratio η_{inh} is introduced to characterize the amplitude inhibition of all the electromagnetic force components mentioned in Table 1-4 by using concentric unequal-turn winding.

A. RADIAL FLUX DENSITY OF IM UNDER DIFFERENT CASES

The FFT decomposition result of the air-gap flux density under different cases are performed, as shown in Fig.4. According to the distribution of harmonic flux density by setting supply as sinusoidal and containing low-order harmonics, the amplitude of harmonics flux density of 5th and 7th are increased by 9.68% and 0.85% under full-load condition, 31.76% and 10.05% under no-load condition respectively. With no-load and full-load conditions, the concentric and unequal-turn winding can effectively suppress harmonic flux density. Compared with the case that the supply contains low-order harmonics, the winding has more significant inhibition effect under full-load condition, the suppression of harmonics amplitude of the order 5 and 7th are 68.53% and 64.12% under full-load condition while 49.35% and 17.52% under no-load condition, respectively. Therefore, the double-layer concentric uneven-turns winding can effectively suppress the surge of harmonic amplitude of flux density caused by the low-order supply harmonics especially under full-load condition.

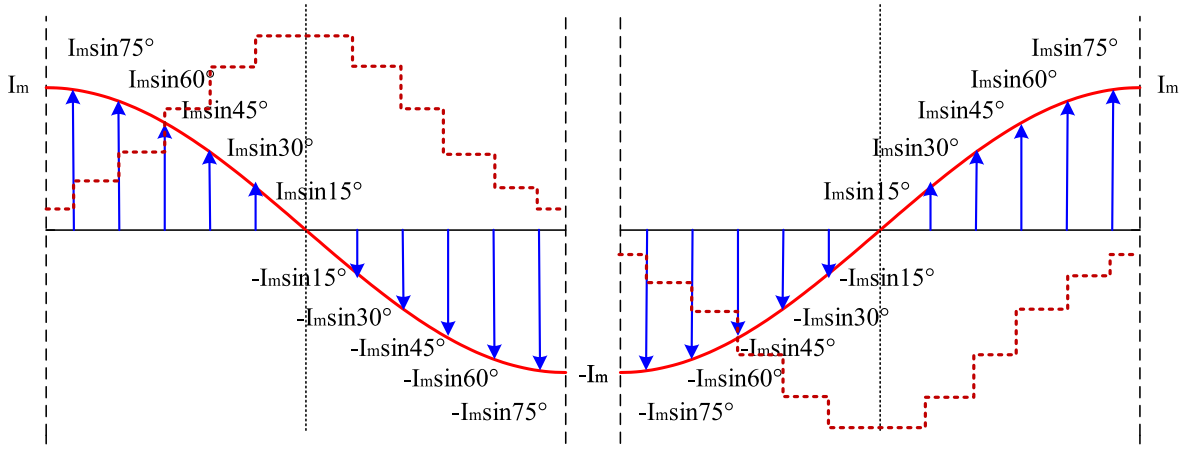

FIGURE 2. Current layer and induced MMF.

B. VARIATION RATIO OF RADIAL ELECTROMAGNETIC FORCE UNDER DIFFERENT CASES

The time-space distribution of radial electromagnetic force is obtained by 2D decomposition, the force amplitudes corresponding to Case #1, Case #2 and Case #3 under no-load and full-load condition are obtained respectively. Since the amplitude variation of force with different orders are disparity obviously, and the simple analysis of force components variation is hard to make intuitive comparison, a method considering reference value is defined to sort the additional force introduced by low-order supply harmonics according to the space order. The ratio of amplitude increments of force in low-order supply harmonics and the ratio of force suppression in concentric and unequal-turn winding are calculated respectively according to (6) and (7), by which the reference basis for analysis is unified.

$$\eta_{inc} = \frac{F_{Case\#1} - F_{Case\#2}}{F_{Case\#1}} \times 100\% \tag{6}$$

$$\eta_{inh} = \frac{F_{Case\#2} - F_{Case\#3}}{F_{Case\#2}} \times 100\% \tag{7}$$

where η_{inc} is the increase ratio of force amplitude; η_{inh} is the inhibition ratio of force amplitude; $F_{\text{Case\#1}}$, $F_{\text{Case\#2}}$, $F_{\text{Case\#3}}$ are the force amplitudes corresponding to Case#1, Case#2 and Case#3. The amplitude increment and inhibition ratio of force with different spatial orders are shown in Fig 5.

Fig.5 contains all the force component from the tabulated analysis results in (5). The force groups are divided into order 0, order ±2 and order ±4. The increment of force under Case#2 and inhibition of force under Case#3 are observed respectively. From the results of full-load and no-load conditions, the parallelism degree of distortion ratio of force with order 0, order −2 and order ± 4 is favorable while the dispersion of force with order 2 is significant, with the maximum increment ratio of 3.88% and inhibition ratio of 9.45% respectively. Therefore, the change of force of order 2 and order-4 are more sensitive to the load condition.

According to the increment ratio of force amplitude, when supply contains low-order harmonics, the force increases relative to the sinusoidal supply, with the maximum increment of 2.63%. However, with the appalment of concentric and unequal-turn winding, the change phenomenon of the force amplitude in different groups shown great disparity, the amplitude of force with order 0 and ±2 increase slightly and the maximum increment of force amplitude is 7.82% and maintain at 3%-5%. It seems to be contradictory with the vibration-damping phenomenon. However, through the observation of the inhibition ratio of force with order ±4, the force of concentric and unequal-turn winding is significantly inhibited and the inhibition ratio is mainly concentrated in the range of 60%-80%, the maximum inhibition ratio is 91.30%, which is much higher than the increase ratio of lower order force components, so the substantial suppression of ±4 order electromagnetic force is the fundamental reason for the vibration and noise reduction of concentric and unequal-turn winding. By comparing the ratio of force amplitude of different load conditions, supply modes and winding forms, it can be concluded that.

1) Load condition can affect the amplitude of different force groups greatly, from which the order 2 and order −4 are especially sensitive. After applying the concentric and unequal-turn windings, the force groups of order 0 and 2 are more sensitive to the load condition.

2) With low-order harmonic coupling effect, the amplitude increment ratio of all kins of force group are increased, from the trend of which the force groups of order 2 and order −4 change dramatically, and the supply harmonic doesn't introduce other order force components in the low frequency range.

3) Applying the concentric and unequal-turn windings present a phenomenon that the electromagnetic force amplitude of lower order increase slightly, while the electromagnetic force amplitudes of slightly higher order are greatly suppressed.

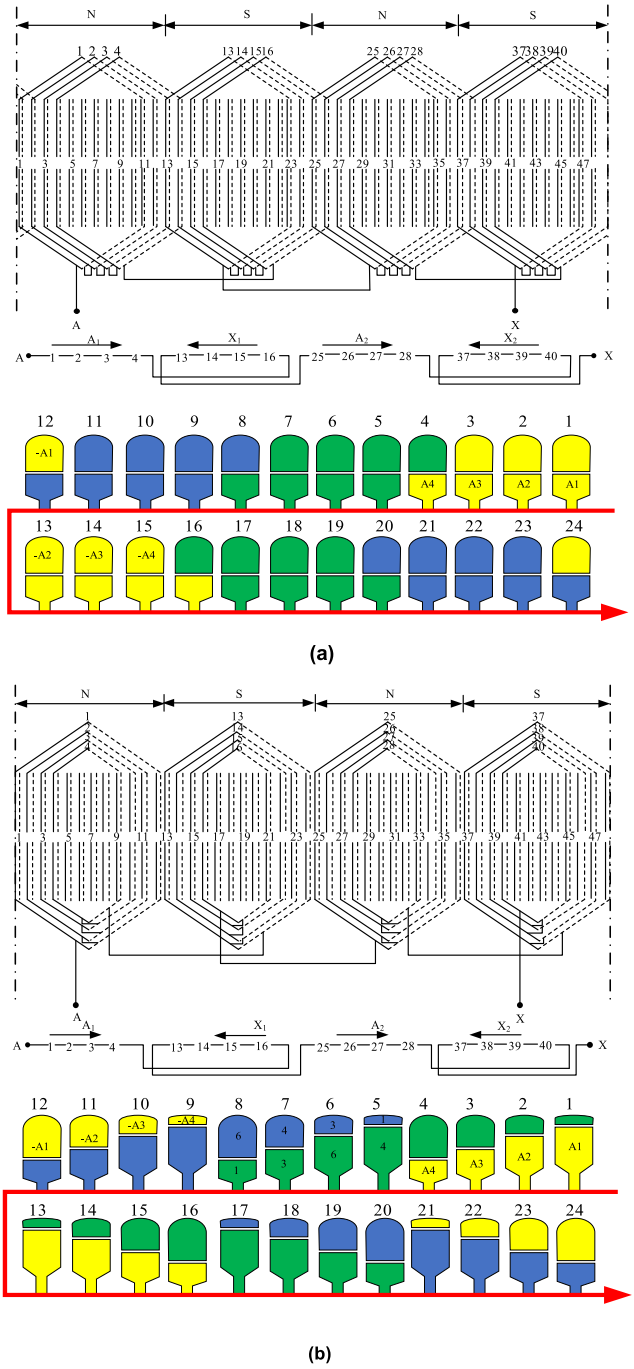

FIGURE 3. Winding structure (a) Ordinary scheme. (b) Low-harmonic scheme.

C. NATURAL FREQUENCY AND HARMONIC RESPONSE ANALYSIS

The modal analysis of motor is carried out to obtain the stator vibration modes and the corresponding natural frequencies. The stiffness parameters of the core material can directly affect the results of the resonance response. The iron core material of the 32kW induction motor is DW350 silicon steel, and the basic rigidity parameters of the material are provided by the manufacturer, as shown in Table 8. modal analysis

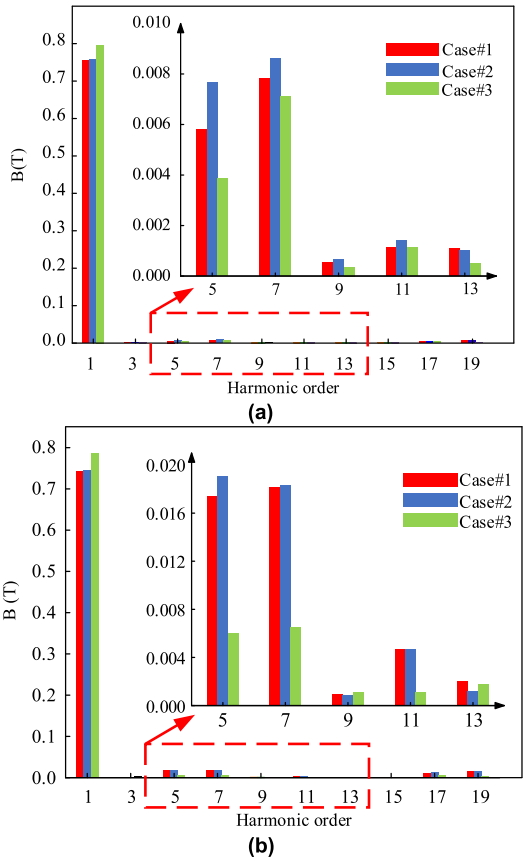

FIGURE 4. FFT decomposition of the air-gap flux density (a) No load; (b) Full load.

TABLE 8. Parameters of Material.

Parameters	Value
Young's modulus(Pa)	2.01×10^{11}
Poisson's ratio	0.3
Density(kg/m^3)	7650

results and the corresponding natural frequencies of order 1 to 4 are shown in Fig.6.

The force corresponding to the natural vibration frequency can induce resonance drastically. Table 1-4 just shows the electromagnetic force with prominent space-time order, in which the force component with time order located near the natural vibration frequency band can cause severe vibration. The amplitude change ratio of each force near natural vibration frequency band under different cases are shown in Fig.7.

According to the variation of force that can cause low-order resonance under different cases, when the supply contains low-order harmonics, each component has a small amplitude increasement under full-load and no-load conditions, the maximum increase ratio is 12.07%. After adopting concentric and unequal-turn winding, the amplitude of force with order ±2 are increased and the maximum increase ratio is 31.48%,

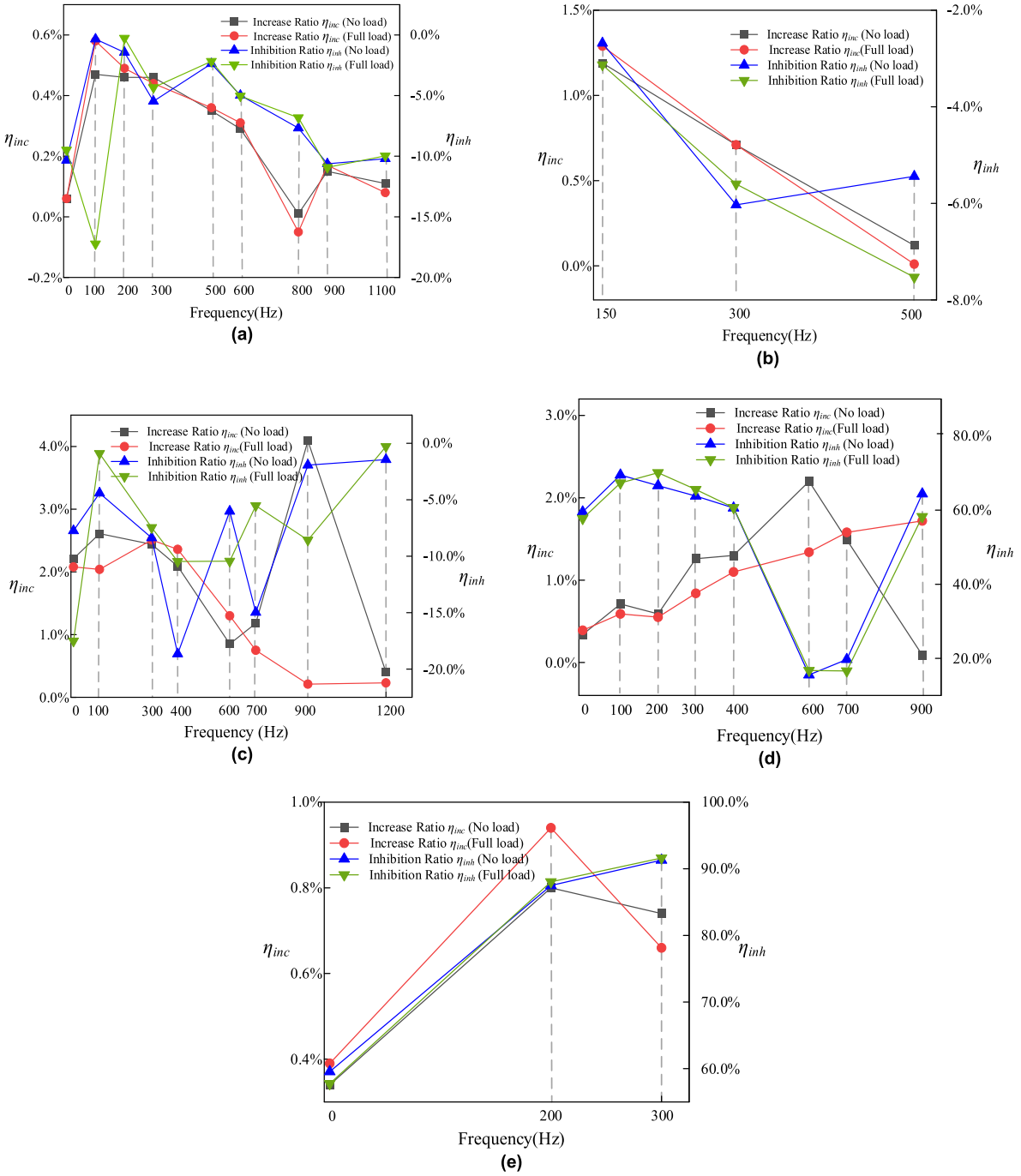

FIGURE 5. Change of force increase ratio and inhibition ratio (a). Group of Order 0. (b). Group of Order -2. (c). Group of Order 2. (d). Group of Order -4. (e). Group of Order 4.

while the force with order ± 4 are significantly suppressed, especially the force with order -4, the highest suppression ratio is 77.46%, the result of which is consistent with the overall analysis of the force group above. Therefore, the special force satisfying the low-order resonance still shows a faint increase in the case of supply containing low-order harmonic. The trend shown that the force amplitude of lower order increase slightly, while the force amplitude of slightly higher order is greatly suppressed.

D. HARMONIC RESPONSE ANALYSIS OF DIFFERENT CASES

The results of harmonic response analysis of the above three cases are shown in Figs. 8 (a) and (b). From the no-load vibration acceleration spectrum, low harmonic supply mainly affects the amplitude of vibration acceleration within the frequency band of 0Hz to 3000Hz in which the highest increase ratio is 799.28%. Meanwhile, the structure of concentric and unequal-turn winding has the most significant inhibition

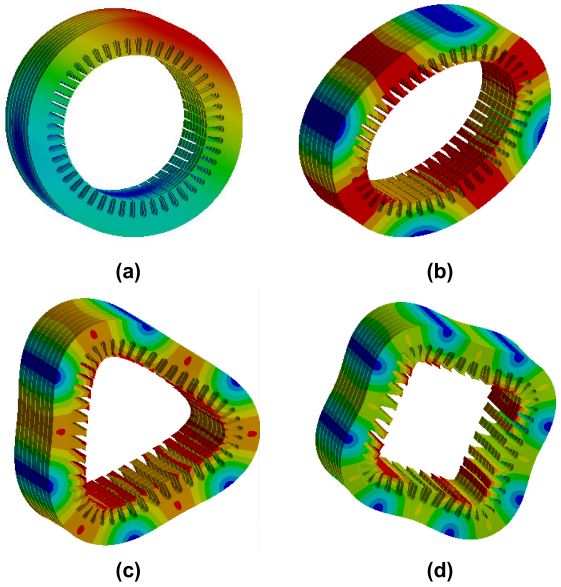

FIGURE 6. Modal analysis results of order 1 to 4. (a). Order 1 (588Hz). (b). Order 2 (850Hz). (c). Order 3 (1644Hz). (d). Order 4 (2939Hz).

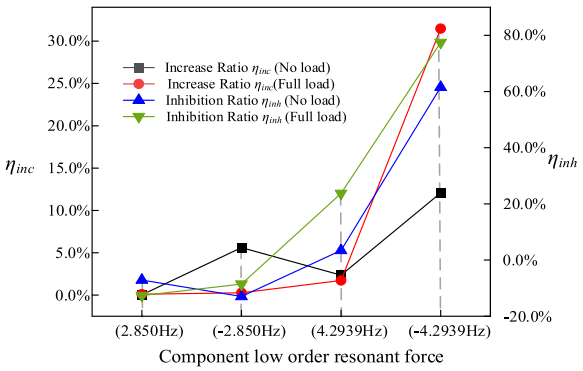

FIGURE 7. Variation of force related to low-order resonant.

effect on vibration acceleration in this frequency band and the highest inhibition ratio is 91.93%. The suppression ratio of 2900Hz is 27.68%. From the vibration acceleration spectrum of full-load condition, low-order supply harmonic mainly affects the amplitude of vibration acceleration in the frequency band of 1400Hz to 1700Hz, in which the highest increase ratio is 758.29%. The suppression effect of concentric and unequal-turn winding is not as well as the no-load condition especially in the range of 0 to 1000Hz. Based on the spectrum distribution, it can be concluded that.

1) From the vibration acceleration spectrum of 0-3000Hz, supply containing low-order harmonic has significant influence on the amplitude of acceleration especially in the frequency band of 0-2500Hz, and the increase acceleration amplitude of some special frequencies too high to be ignored.

2) Concentric and unequal-turn winding has corresponding frequency limitations on the suppression of motor vibration acceleration, application result show that it is prominent in frequency band of 1000-2000Hz and the effect under no-load

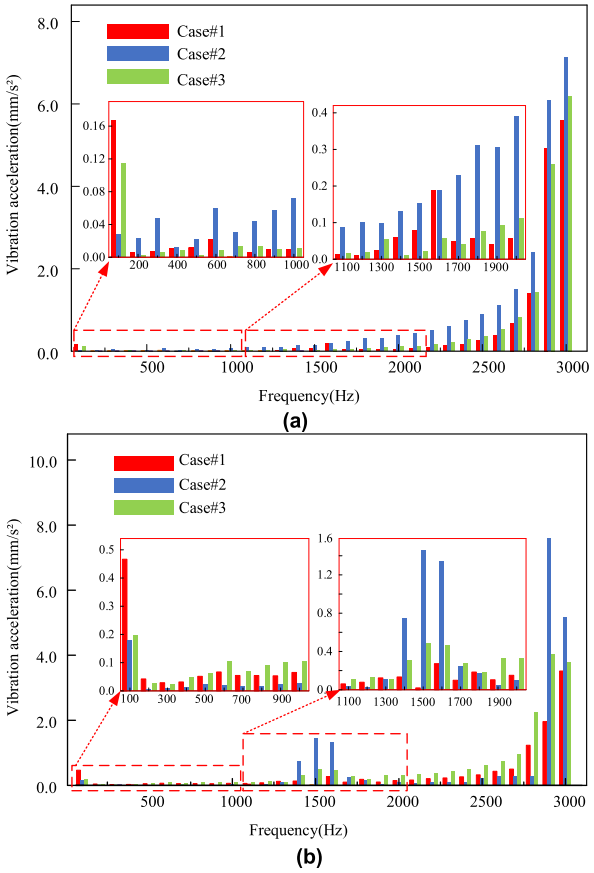

FIGURE 8. Spectrum of harmonic response. (a). 0-3000 Hz, no-load. (b). 0-3000 Hz, full-load.

condition is obviously better than the effect under full-load condition.

3) For the peak value of vibration acceleration caused by the 4th order resonance, the concentric and unequal-turn winding has a good inhibition effect no matter under no-load and full-load conditions.

V. EXPERIMENTAL VALIDATION

The manufactured concentric and unequal-turns winding are shown in Fig 9. For the rated power 32-kW IM, with the original winding and the concentric and unequal-turn winding are adopted respectively, the vibration test bench is shown in Fig 10, the test prototype, vibration signal test platform and high-precision supply harmonic measuring device are shown in (a), (b) and (c) respectively. In accordance with the simulation scheme, the supply mode of motor is power frequency power supply and the filter device is set on the supply side. The vibration sensor used in the test is B&K 4535-B and the data analysis device is Data Acquisition and Signal Processing test system (DASP), which is a multi-channel signal acquisition and real-time analysis multifunctional software operating on the Windows platform.

P-1 and P-2 are the 2 measured positions of stator frame bottom, and the output result of the sensor is acoustic signal,

FIGURE 9. Concentric unequal turns winding and embedding process.

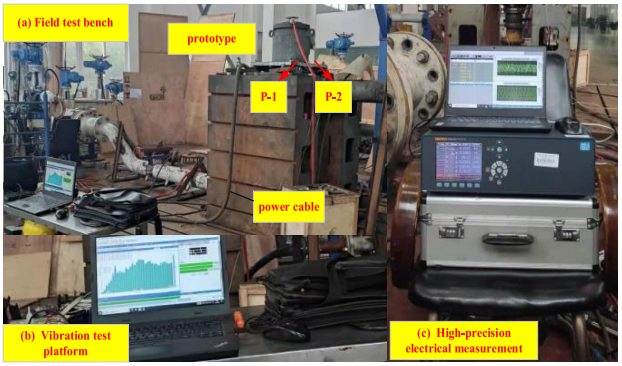

FIGURE 10. Field test.

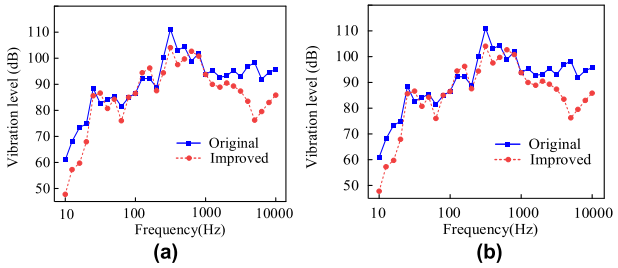

FIGURE 11. Test results. (a). P-1. (b). P-2.

TABLE 9. Experimental Results.

	Point 1	Point 2	Ave
Original (dB)	90.3	89.1	89.7
Improved (dB)	86.5	87.3	86.9

which is represented by the acoustic radiation power and can be converted through vibration acceleration [22], the corresponding acoustic radiation power of P-1 and P-2 are shown in Fig 11. The average vibration levels of each position and the total vibration level are given in Table 9. It can be seen that.

1) The vibration in the frequency band of 300-1000 Hz reflects a good suppression effect, while the test results of different measuring points are showing great difference in the frequency band of 10-50 Hz.

2) For the high frequency band, that is the frequency is more than 3000 Hz, the vibration level suppression effect is more prominent.

3) From the perspective of vibration level, the concentric and unequal-turn winding has different degrees of suppression effect on the average vibration level of the two sampling points, and the maximum suppression ratio is 6.22%. The overall vibration level suppression of the concentric and unequal-turn winding scheme is 2.8 dB, which is reasonable compared with the results of other motor vibration test.

VI. CONCLUSION

This study investigates the vibration characteristics of IM considering supply with low-order harmonics, and a concentric and unequal-turn winding is also proposed to suppress the vibration. Main conclusions are as follows:

1) The characteristics of air gap flux density and radial force of IM with low-order harmonic are studied. The ratio of force change is firstly introduced to evaluate the change of force characteristic between different cases.

2) To suppress unconventional vibration of IM caused by low-order supply harmonics effectively, a cost-efficiency low- harmonic winding design scheme aims at minimizing the coefficient of harmonic winding is proposed and the influence in different frequency bands is investigated.

3) Experimental validation on a 32-kW IM is performed, the results show that the overall vibration level suppression of the concentric and unequal-turn winding scheme is 2.8 dB.

REFERENCES

[1] Z. Q. Zhu and D. Howe, "Instantaneous magnetic field distribution in brushless permanent magnet DC motors. III. Effect of stator slotting," *IEEE Trans. Magn.*, vol. 29, no. 1, pp. 143–151, Jan. 1993.

[2] J. P. Lecointe, R. Romary, J. F. Brudny, and M. McClelland, "Analysis and active reduction of vibration and acoustic noise in the switched reluctance motor," *IEE Proc. Electr. Power Appl.*, vol. 151, no. 6, p. 725, 2004.

[3] D. Zarko, D. Ban, and T. A. Lipo, "Analytical calculation of magnetic field distribution in the slotted air gap of a surface permanent-magnet motor using complex relative air-gap permeance," *IEEE Trans. Magn.*, vol. 42, no. 7, pp. 1828–1837, Jul. 2006.

[4] R. Islam and I. Husain, "Analytical model for predicting noise and vibration in permanent-magnet synchronous motors," *IEEE Trans. Ind. Appl.*, vol. 46, no. 6, pp. 2346–2354, Nov. 2010.

[5] D. Torregrossa, B. Fahimi, F. Peyraut, and A. Miraoui, "Fast computation of electromagnetic vibrations in electrical machines via field reconstruction method and knowledge of mechanical impulse response," *IEEE Trans. Ind. Electron.*, vol. 59, no. 2, pp. 839–847, Feb. 2012.

[6] R. Yacamini and S. C. Chang, "Noise and vibration from induction machines fed from harmonic sources," *IEEE Trans. Energy Convers.*, vol. 10, no. 2, pp. 286–292, Jun. 1995.

[7] F. Lin, S. Zuo, W. Deng, and S. Wu, "Modeling and analysis of electromagnetic force, vibration, and noise in permanent-magnet synchronous motor considering current harmonics," *IEEE Trans. Ind. Electron.*, vol. 63, no. 12, pp. 7455–7466, Dec. 2016.

[8] M. Tsypkin, "The origin of the electromagnetic vibration of induction motors operating in modern industry: Practical experience—Analysis and diagnostics," *IEEE Trans. Ind. Appl.*, vol. 53, no. 2, pp. 1669–1676, Mar. 2017.

[9] J. Du, Y. Li, Z. Yu, and Z. Wang, "Research on radial electromagnetic force and vibration response characteristics of squirrel-cage induction motor fed by PWM inverter," *IEEE Trans. Appl. Supercond.*, vol. 31, no. 8, pp. 1–4, Nov. 2021.
[10] S. Wang, J. Hong, Y. Sun, and H. Cao, "Effect comparison of zigzag skew PM pole and straight skew slot for vibration mitigation of PM brush DC motors," *IEEE Trans. Ind. Electron.*, vol. 67, no. 6, pp. 4752–4761, Jun. 2020.
[11] C. Wang, X. Bao, S. Xu, Y. Zhou, W. Xu, and Y. Chen, "Analysis of vibration and noise for different skewed slot-type squirrel-cage induction motors," *IEEE Trans. Magn.*, vol. 53, no. 11, pp. 1–6, Nov. 2017.
[12] L. Wang, X. Bao, C. Di, and Y. Zhou, "Influence on vibration and noise of squirrel-cage induction machine with double skewed rotor for different slot combinations," *IEEE Trans. Magn.*, vol. 52, no. 7, pp. 1–4, Jul. 2016.
[13] M. Rahmani, A. Darabi, and F. P. Deylami, "Impact of the stator coil pitch on acoustic noise and vibration of squirrel cage induction motors," *IEEE Trans. Energy Convers.*, vol. 38, no. 4, pp. 2344–2352, Dec. 2023.
[14] X. Chen, J. Wang, and V. I. Patel, "A generic approach to reduction of magnetomotive force harmonics in permanent-magnet machines with concentrated multiple three-phase windings," *IEEE Trans. Magn.*, vol. 50, no. 11, pp. 1–4, Nov. 2014.
[15] A. Sun, J. Li, R. Qu, and D. Li, "Effect of multilayer windings on rotor losses of interior permanent magnet generator with fractional-slot concentrated-windings," *IEEE Trans. Magn.*, vol. 50, no. 11, pp. 1–4, Nov. 2014.
[16] P. B. Reddy, A. M. EL-Refaie, and K.-K. Huh, "Effect of number of layers on performance of fractional-slot concentrated-windings interior permanent magnet machines," *IEEE Trans. Power Electron.*, vol. 30, no. 4, pp. 2205–2218, Apr. 2015.
[17] X. Rao, L. Rong, W. Gan, C. Xiao, and Y. Zhou, "Investigation of noise sources in fractional-slot concentrated winding motors considering high-order radial/tangential electromagnetic force combination and modulation," *IEEE Access*, vol. 11, pp. 143980–143997, 2023.
[18] A. S. Abdel-Khalik, S. Ahmed, and A. M. Massoud, "Effect of multilayer windings with different stator winding connections on interior PM machines for EV applications," *IEEE Trans. Magn.*, vol. 52, no. 2, pp. 1–7, Feb. 2016.
[19] H. Zhao, Z. Zhou, Z. Wang, J. Kang, H. H. Eldeeb, G. Xu, Y. Zhan, and Y. Zhang, "Vibration characteristics of induction motor considering the lower-order harmonics in power supply," in *Proc. IEEE Energy Convers. Congr. Expo. (ECCE)*, Detroit, MI, USA, Oct. 2022, pp. 1–5, doi: 10.1109/ECCE50734.2022.9947938.
[20] S. Wu, W. Tong, W. Li, S. Yu, and R. Tang, "Electromagnetic vibration analysis of high-speed permanent magnet synchronous machines with amorphous metal stator cores considering current harmonics," *IEEE Trans. Ind. Electron.*, vol. 67, no. 12, pp. 10156–10167, Dec. 2020.
[21] S. K. Chen, *Motor Design*. Beijing, China: Machinery Industry Press, 2008, pp. 191–196.
[22] J. F. Gieras, *Noise of Polyphase Electric Motors*. Boca Raton, FL, USA: CRC Press, 2006, pp. 6–10.

XUANDONG WU received the B.E. degree in electric machines and apparatus from Shanghai Jiao Tong University, Shanghai, China, in 1990.

He is currently a Professor Level Senior Engineer with Wolong Electric Nanyang Explosion Group Company Ltd., Nanyang, Henan. His research interests include electromagnetic optimization, thermal management and mechanical design of explosion-proof motors, synchronous generators/condensers, and special motors.

LIMIN DIAO received the B.E. degree in electrical machines and apparatus from Shenyang University of Technology (SUT), Shenyang, China, in 2003, and the M.E. degree in electrical machines and apparatus from North China Electric Power University (NCEPU), Beijing, China, in 2018.

He is currently a Senior Engineer with Harbin Electric Power Equipment Company Ltd., Harbin, Heilongjiang. His research interests include multi-physics analysis of electrical appliances and special motor design.

ZIXU WANG (Student Member, IEEE) received the B.E. degree in electrical engineering from Jiangsu University, Zhenjiang, China, in 2021. He is currently pursuing the master's degree in electrical engineering with the School of Electrical and Electronic Engineering, North China Electric Power University (NCEPU).

His research interests include multi-physics analysis of electrical machines, design and optimization of high efficiency, and low vibration motors.

SHAN WANG received the B.E. degree in electrical engineering from the Qilu University of Technology, Jinan, China.

He is currently a Senior Engineer with Dezhou Hengli Electrical Machinery Company Ltd., Dezhou, Shandong. His research interests include design and optimization of low vibration and noise motors.

HAISEN ZHAO (Senior Member, IEEE) received the B.E. degree in agricultural electrification and automation from the Agriculture University of Hebei, Baoding, China, in 2004, and the M.E. and Ph.D. degrees in electric machines and apparatus from North China Electric Power University (NCEPU), Beijing, China, in 2007 and 2011, respectively.

He is currently a Professor with the School of Electrical and Electronic Engineering, NCEPU. He is the author or coauthor of more than 150 papers in peer-reviewed journals and major international conferences. Furthermore, he has 24 patents awarded in the area of electric machine design, control, and energy-saving technologies. His research interests include electrical motors design, diagnosis, energy analysis, energy-saving technologies of electric machines and drive systems, and wireless power transfer.

Dr. Zhao is a fellow of the Institute of Engineering and Technology (IET).